PHYSICAL REVIEW B **76**, 184505 (2007)

Interface electronic structure, two-dimensional metallicity, and possible interface superconductivity in CuCl/Si superlattices

S. H. Rhim,[1,*] R. Saniz,[1] Jaejun Yu,[2] Lin-Hui Ye,[1] and A. J. Freeman[1]
[1]*Department of Physics and Astronomy, Northwestern University, Evanston, Illinois 60208, USA*
[2]*CSCMR and Department of Physics and Astronomy, Seoul National University, Seoul 151-747, Korea*

(Received 18 June 2007; published 6 November 2007)

Results of highly precise all-electron full-potential linearized augmented plane wave density functional calculations demonstrate (i) two-dimensional metallicity, and (ii) possible superconductivity in CuCl/Si superlattices for [111] and [001] directions. The feature of two-dimensional (2D) metallicity arises from the charge transfer at the interfaces between CuCl and Si, where there is the valence charge imbalance. The 2D features are well evidenced by band structure, Fermi surfaces, and charge densities. Furthermore, to investigate possible superconductivity, we use McMillan [Phys. Rev. **167**, 331 (1968)] formula to estimate T_C, and evaluate the electron-phonon coupling constant, λ, using the rigid muffin-tin approximation. From our calculations, it is the interfaces that contribute to all intriguing physics: 2D metallicity, charge transfer, nonvanishing Hopfield [Phys. Rev. **186**, 443 (1969)] parameter, and electron-phonon coupling. Moreover, our T_C estimations (0.03–4.40 K) reveal that the electron-phonon coupling is too weak to account for the high T_C (60–150 K) suggested in early experiments.

DOI: 10.1103/PhysRevB.76.184505 PACS number(s): 74.78.Fk, 73.20.−r

I. INTRODUCTION

Recent advances in materials synthesis and epitaxial growth techniques have attracted much interest in the physics of heterointerfaces between materials with either different polarities or oxidation states. Polarity discontinuity in semiconductor heterointerfaces such as GaAs/Ge [001] (Refs. 1–3) or III-V alloys on Si [001] (Ref. 4) has been well studied. As for oxide heterointerfaces, the layer-by-layer growth of the $LaTiO_3/SrTiO_3$ and $LaAl_3/SrTiO_3$ superlattices has attracted recent attention.[5–8] Despite the fact that these consist of two insulators in their bulk form, metallic conductivity was observed in the experiments.[5,7]

Actually, interest in superlattices and heterointerfaces goes back several decades ago. A possible superconducting state in a metal sandwiched by dielectric materials was proposed in the early 1960s based on the so-called "excitonic mechanism" of superconductivity,[9,10] where it was suggested that a higher transition temperature (T_C) might be achieved by excitonic mediation. Several geometries were suggested as candidates for the excitonic mechanism: (a) metallic "chains" or strings with polarizers placed alongside them[9] and, (b) dielectric-metal-dielectric sandwiches, where the conduction electron states are surrounded by a dielectric medium.[10] The dielectric-metal-dielectric geometry was studied theoretically by Allender, Bray, and Bardeen (ABB)[11] with a single metal-dielectric interface. Following ABB, some experimental efforts to observe superconductivity in several systems include (a) clean PbTe surfaces,[12] (b) ultrathin Al films on Si,[13] (c) eutectic alloys[14] (Al-Ge and Al-Si), and (d) ultrathin Pb, In, and Tl layers deposited on PbTe,[15] but superconductivity was not confirmed in any of them. However, nearly ideal diamagnetism was observed in bulk CuCl by Brandt *et al.*[16] and Chu *et al.*[17] Shortly thereafter, Abrikosov proposed the formation of "metallic excitonium"[18,19] to explain their observation, but again this was never fully confirmed. Later, Mattes and Foiles studied epitaxially grown CuCl on a Si [111] substrate.[20] They found that it is diamagnetic when the applied field is perpendicular to the interface while it is paramagnetic when the applied field is parallel to the interface. Moreover, the diamagnetism was nearly ideal between 60 and 150 K. In a following work, Mattes speculated further on the possible superconducting origin of the observation because of a sudden drop of resistivity by 5 orders of magnitude at 77 K.[21]

After the work by Mattes and Foiles, a preliminary first-principles investigation on the possible interfacial superconductivity in CuCl/Si was reported by Yu and Freeman.[22] From the results of electronic structure calculations with a $(CuCl)_1/(Si)_4$ superlattice model, the existence of two-dimensional (2D) metallic states at the interface was considered to be highly plausible. The present work is a continuation and extension of this first study. We consider first the [111] superlattices $(CuCl)_n/(Si)_{4n}$, with $n=1$ to $n=3$.[23] We also consider [001] superlattices, $(CuCl)_n/(Si)_m$,[24] with $(CuCl)_2/(Si)_8$ [2/8], $(CuCl)_4/(Si)_8$ [4/8], and $(CuCl)_4/(Si)_{12}$ [4/12]. The presence of 2D metallic states localized at the CuCl/Si interfaces is confirmed from band structures, Fermi surfaces, and charge densities. Thus, the CuCl/Si superlattice can be viewed not only as the heterointerfaces of two different semiconductors but also as the dielectric-metal-dielectric sandwich structure suggested by Ginzburg.[10]

As a step toward understanding the physics of the interface metallic states and to investigate a possible superconductivity at the CuCl/Si heterointerface, we carried out first-principles electronic structure calculations for the CuCl/Si superlattices using the highly precise all-electron full-potential linearized augmented plane wave (FLAPW) method,[25,26] and also estimated T_C considering the electron-phonon mechanism. In Sec. II, the geometry of the [111] and [001] CuCl/Si superlattices and computational details are described. Next, results for relaxed superlattices are discussed in Sec. III A. The two-dimensional metallicity is pre-

©2007 The American Physical Society

sented in Sec. III B, along with an analysis of the band structure, Fermi surfaces, and charge densities, and the projected density of states (pDOS) of the superlattices around E_F is provided to identify conduction carriers. These comparisons give a basic idea as to how the bonding character is changed. Interface charge of superlattices is discussed in Sec. III D. Finally, in Sec. IV, to discuss the possible superconductivity in these superlattices, T_C is estimated using the conventional electron-phonon interaction in the crude rigid muffin-tin approximation (RMTA).[27] Most of the electron-phonon coupling responsible for superconductivity is present at the interfaces, and results in a T_C of 0.03–4.40 K

II. METHODS

CuCl and Si crystallize in the zinc-blende and diamond structures, respectively, with similar lattice constants, 5.42 Å (CuCl) and 5.43 Å (Si). For the [111] case, the superlattice is constructed to satisfy the periodicity along the [111] direction in the zinc-blende structure for the $n=1$ and 3 cases. The crystal structure is shown schematically in Fig. 1 for the $n=3$ case with their hexagonal lattices in the *ab* plane. For the [001] case, on the other hand, the superlattice forms a square lattice in the *ab* plane as shown in Fig. 2.[28] Four atomic layers are one unit of the *c* direction periodicity, which results in $(\mathrm{CuCl})_n/(\mathrm{Si})_m$.[29] We performed structural optimizations, i.e., of internal coordinates for each volume and each c/a, for all cases, and we employed the highly precise FLAPW[25,26] method in the local density approximation, with the exchange-correlation potential formulated by Hedin and Lundqvist.[30] We used muffin-tin (MT) radii of 2.15 a.u. (Cu), 2.00 (Si and Cl), and spherical harmonics with $\ell \leq 8$ inside the MT spheres. The cut-off energy of the plane wave basis is 7.22 htr, while that of the potential representations are 103.68 and 72.0 htr for the [111] and the [001] cases, respectively. The improved tetrahedron method[31] is used for *k* point integrations, with 119 ($n=1,3$), 98 (2/8), 128 (4/8), and 243 (4/12) points in the irreducible Brillouin zone. The optimized lattice constants for all superlattices are tabulated in Table I, where the numbers in parentheses are the change (in %) relative to those of the bulk zinc-blende structure.[32]

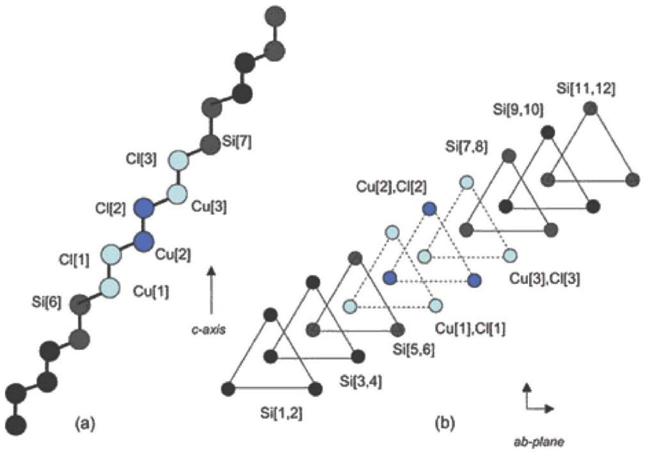

FIG. 1. (Color online) Schematic drawing of the $n=3$ CuCl/Si superlattice: (a) side view and (b) top view.

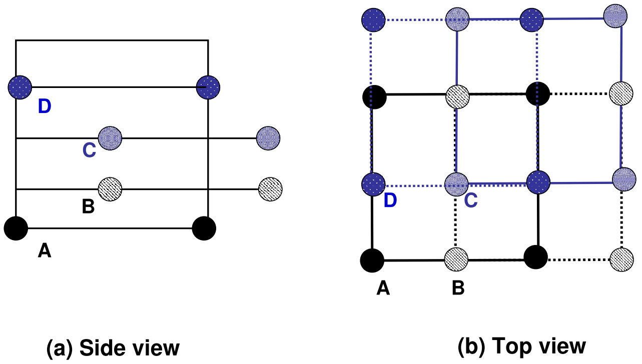

FIG. 2. (Color online) Schematic drawing of the [001] CuCl/Si superlattice: (a) side view of one zinc-blende cell, and (b) top view. Stacking order is A-B-C-D type as indicated in figure, and represent, e.g., Si[1], Si[2], Si[3], and Si[4], or Cu[1], Cl[1], Cu[2], and Cl[2].

III. RESULTS

Here we show in detail the band structure and Fermi surfaces (FSs), as well as the density of states (DOS) around E_F. Then we discuss charge transfer in relation to the origin of the 2D metallic states at both the Cu/Si and Cl/Si interfaces.

A. Structural relaxation

The layer-by-layer distances after relaxation with the optimized lattice constant, *a*, and the c/a ratio are compared with those of the zinc-blende structure with the optimized *a* and c/a. The percentage changes of layer distance are tabulated in Table II for the [111] case and in Table III for the [001] case.

First, in the [111] superlattices, the Si-Si layer distance changes are within 5% relative to the zinc-blende structure, but are much larger for the other layers: in the $n=1$ case, the Si[3]-Cl, Cu-Si[2], and Cu-Cl distance changes indicate that the Cl/Si and Cu/Si interfaces are strongly affected by relaxation, suggesting that an increase of bonding between them occurs with relaxation, while the Cu–Cl bonding is weakened. In the $n=3$ case, the Si[7]-Cl[3] distance change is much larger than the Cu[1]-Si[6] distance change. The

TABLE I. Optimized lattice constants (a) and c/a ratio for the superlattices. For the [111] superlattices, lattice constants are converted to those of zinc blende. The numbers in parentheses are the relative change (in %) of a and c/a to those of the zinc-blende structure without relaxation.

	$n=1$	$n=3$	2/8	4/8	4/12
a(Å)	5.59 (3.06%)	5.44 (0.45%)	5.38 (−0.8%)	5.30 (−2.22%)	5.34 (−1.45%)
c/a	2.28 (−7.02%)	7.06 (−3.99%)	3.02 (+0.77%)	4.16 (+3.92%)	5.11 (+6.83%)

TABLE II. The [111] superlattice: percentage change of layer distances before and after relaxation. The changes of layer distances not listed are less than 5%.

$n=1$	Change (%)	$n=3$	Change (%)
Si[4]-Si[3]	5.14	Si[7]-Cl[3]	−30.75
Si[3]-Cl	−39.27	Cl[3]-Cu[3]	7.13
Cl-Cu	15.69	Cu[3]-Cl[2]	−41.97
Cu-Si[2]	−33.51	Cl[2]-Cu[2]	11.65
Si[2]-Si[1]	4.00	Cu[2]-Cl[1]	−56.83
Si[1]-Si[4]	1.71	Cl[1]-Cu[1]	10.38
		Cu[1]-Si[6]	−6.61

Cu-Cl distance changes in the CuCl region are driven by the increase of the Cu-Cl distance in the bonds along the [111] direction.

Second, in the [001] superlattices, the Cl-Si layer distance increases by 6.7%, 43.8%, and 43.9%, for the 2/8, 4/8, and 4/12 cases, respectively; the Cu-Si distances decrease by much less than in the [111] case and are not as systematic. However, the fact that the CuCl region is more affected than the Si region is similar to that of the [111] superlattices.

B. Two-dimensional metallic states

The band structures for the two growth directions, i.e., [111] and [001] superlattices, are shown in Figs. 3 and 6, respectively. It is notable that metallic states are found in both cases to arise from two semiconductors with band gaps 3.4 eV (CuCl) and 1.14 eV (Si) in their bulk. In the [111] superlattices, two bands cross E_F, where the hole (electron) band is labeled as $h(e)$ in Fig. 3. The character of the hole band is mostly Cu(d)-Si(p), while that of the electron band is mostly Cl(p)-Si(p), which clearly characterizes and distinguishes the two interfaces: in the $n=1$ case, one can see a tendency to low dispersion along the M-L and A-Γ directions; in the $n=3$ case, the dispersion along these directions almost vanishes, indicating strong two dimensionality.

The Fermi surfaces of the [111] superlattices are depicted in Fig. 4. The inner sheet from the hole band (labeled as h) forms an open cylindrical shape centered at the Γ point, while the outer sheets from the electron band (labeled as e) are located at the corners of the Brillouin zone. For $n=1$, the electron band sheet is connected, whereas for $n=3$ there are multiple sheets. The low dispersion of the Fermi surfaces along the c direction reflects the two dimensionality of the superlattices, and the 2D interface metallicity is further illustrated in a charge density plot (cf. Fig. 5). For the charge density, only the electronic states within an energy slice of 0.025 eV below E_F are taken into account. In both the $n=1$ and $n=3$ cases, most of the charge is located at the Cu/Si and Cl/Si interfaces. The 2D character of the conducting charge is clearly manifested in the $n=3$ case. Note that the superlattice is divided into metallic layers (the Cu/Si and the Cl/Si interfaces) and dielectric regions (the CuCl and the Si regions).

TABLE III. The [001] superlattice: percentage changes of layer distances before and after relaxation. The changes of layer distances not listed are less than 5%.

Layer	2/8	Layer	4/8	4/12
Si[5]-Cl[2]	6.71	Si[5]-Cl[4]	43.84	43.88
Cl[2]-Cu[2]	0.95	Cl[4]-Cu[4]	−10.91	−11.58
Cu[2]-Cl[1]	−16.85	Cu[2]-Cl[1]	−9.99	−11.05
Cl[1]-Cu[1]	15.13	Cl[1]-Cu[1]	11.29	11.74
Cu[1]-Si[6]	−4.31	Cu[1]-Si[6]	−1.00	−0.40

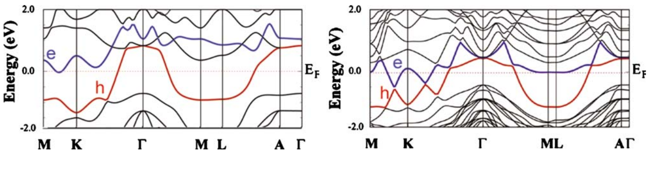

(a) (b)

FIG. 3. (Color online) Band structure of the [111] superlattice: (a) $n=1$ and (b) $n=3$. The hole (electron) band, in red (blue), is labeled as $h(e)$. $L=(\pi/a,0,\pi/c)$ and $A=(0,0,\pi/c)$, respectively.

The band structures of the [001] superlattices are shown in Fig. 6 for the (a) 2/8, (b) 4/8, and (c) 4/12 cases. Again metallic states are found in all cases, where the hole (electron) bands are again labeled as $h(e)$. In the 2/8, two bands cross E_F, while in the 4/8 and the 4/12 cases, three and four bands cross E_F, respectively. The band dispersions in the three cases are similar, but the positions of the bands with respect to E_F are different: compared to the 2/8 case, the electron bands are pushed downward along the X-R line in the two other cases; in contrast, the hole bands are pushed upward along the Γ-Z line. As in the [111] superlattice, the band character is mostly Cu(d)-Si(p) for the hole bands, and Cl(p)-Si(p) for the electron bands. The dispersion along the c direction (along Γ-Z and X-R) is weak but not as weak as in the [111] case for the hole bands, in particular.

The Fermi surfaces of the [001] superlattices are shown in Fig. 7. In the 2/8 case, the inner sheet, which is from the hole band, has a double lip structure symmetric with respect to the Σ-Γ-Σ line, whereas the outer sheet, which is from the electron band, is centered around the corner points (X) and

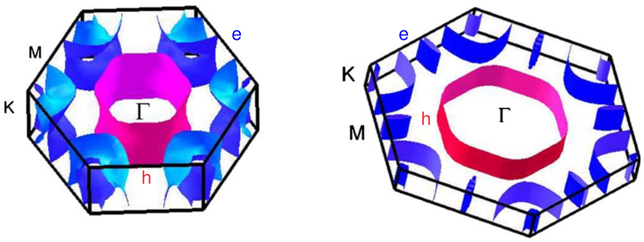

(a) (b)

FIG. 4. (Color online) Fermi surfaces of the [111] superlattice: (a) $n=1$ and (b) $n=3$. Sheets from the hole (electron) band, in red (blue), is located at the zone center (zone corner) and labeled as $h(e)$.

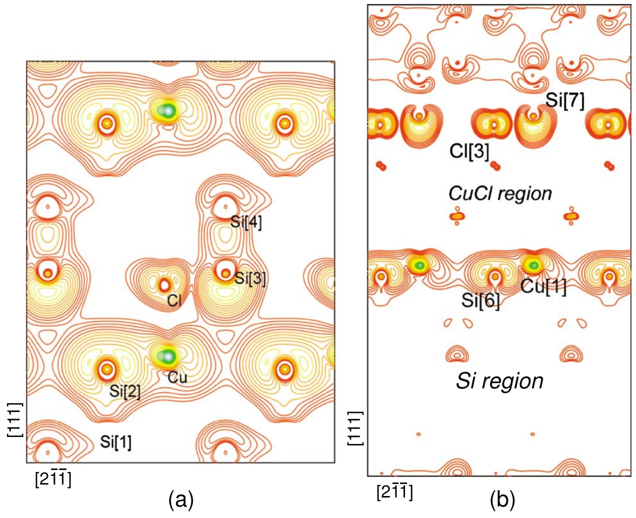

FIG. 5. (Color online) Charge density contour plot of the (a) $n=1$ and (b) $n=3$ superlattices around E_F within an energy slice of 0.025 eV; the starting density is 1.0×10^{-4} e/bohr^3 and subsequent lines increase by a factor of 1.25.

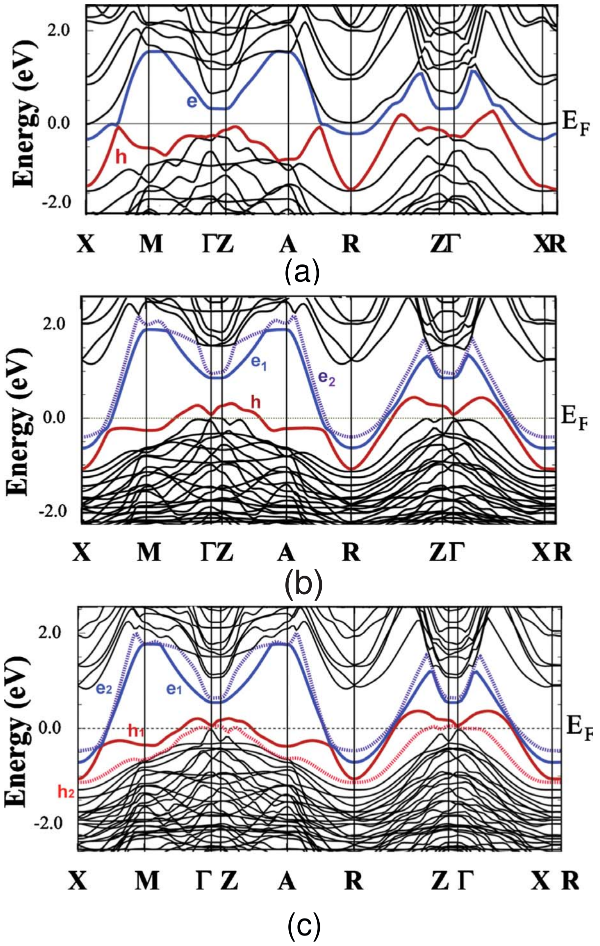

FIG. 6. (Color online) Band structure of the [001] superlattice: (a) 2/8, (b) 4/8, and (c) 4/12. The hole (electron) band, in red (blue), is labeled as $h(e)$. The symmetry points are $M=(\pi/a,\pi/a,0)$, $Z=(0,0,\pi/c)$, $R=X+(0,0,\pi/c)$, and $A=M+(0,0,\pi/c)$, respectively.

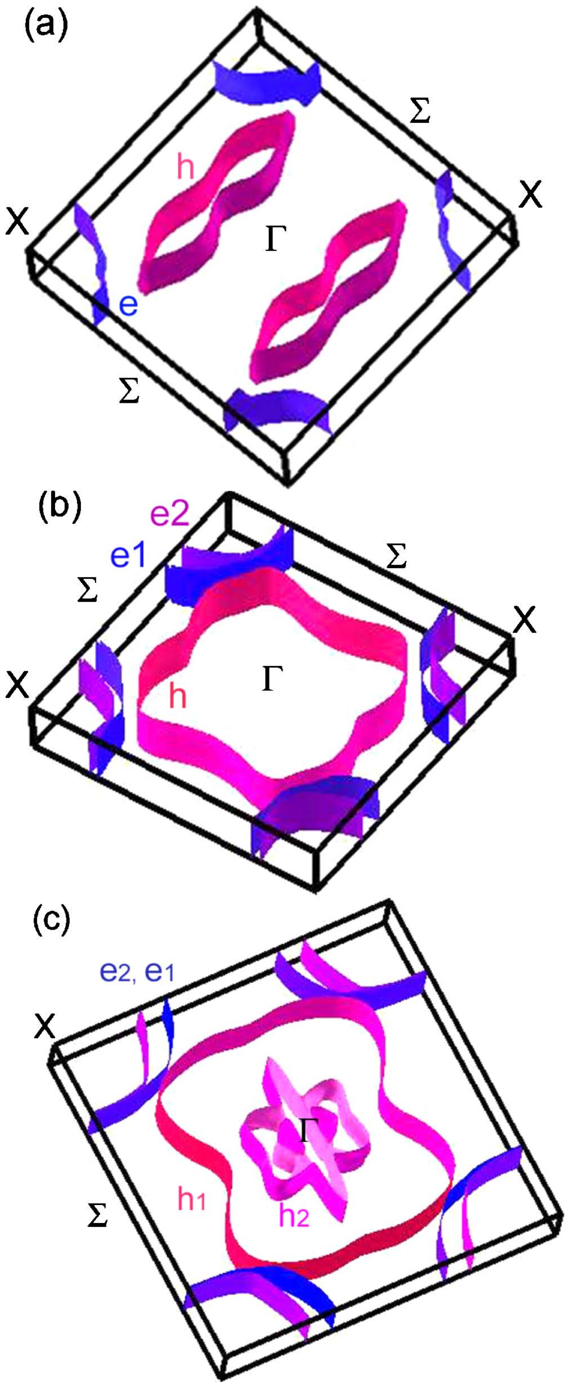

FIG. 7. (Color online) Fermi surfaces of the [001] superlattice: (a) 2/8, (b) 4/8, and (c) 4/12. Sheets from the hole (electron) band, in red (blue) is located at zone center (zone corner) and labeled as $h(e)$. Corner point of the Brillouin zone is denoted by its label, where $\Sigma=M/2=(\pi/2a,\pi/2a,0)$.

parallel along the c direction. In the 4/8 and 4/12 cases, the inner hole band sheet has a simply connected structure centered at Γ, whereas the outer electron band sheets are centered around the corner points (X) and parallel along the c direction, as in the 2/8 case. In the 4/12 case, however, an additional sheet with a connected ribbon shape in the zone center is found, which is from hole band $h2$ in Fig. 6(c). The

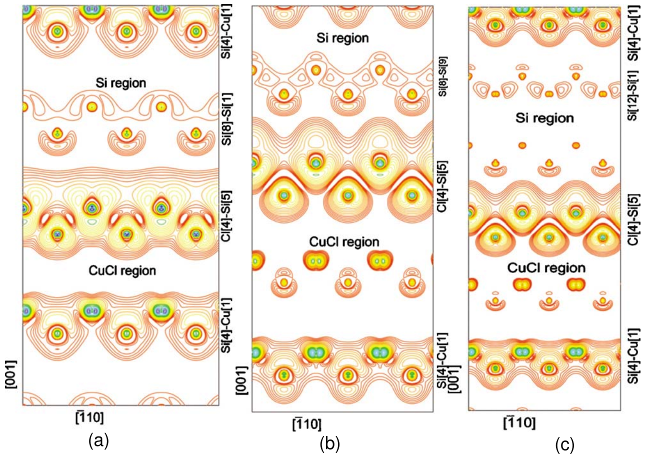

FIG. 8. (Color online) Charge density contour plot of (a) 2/8, (b) 4/8, and (c) 4/12 superlattices around E_F within an energy slice of 0.025 eV. The interface, and CuCl and Si regions are labeled. The starting density is 5.0×10^{-4} e/bohr^3 and subsequent lines increase by a factor of 1.25.

2D character of the [001] superlattices is well manifested in the Fermi surfaces as in the [111] case.

The charge density plot of the [001] superlattice is given in Fig. 8 for the (a) 2/8, (b) 4/8, and (c) 4/12 cases, respectively; the interfaces are labeled for both the Cu/Si and Cl/Si interfaces. Again, most of the charge is found at the interfaces, but is spread out more from the interfaces compared to the [111] case. The metallicity in the Cu/Si interface is confined to the interface, whereas the Cl/Si interface has some conducting charge spread to the Si region. Clearly, in the [001] case as in the [111] case, the interfaces form metallic slabs with the CuCl and Si regions as dielectrics.

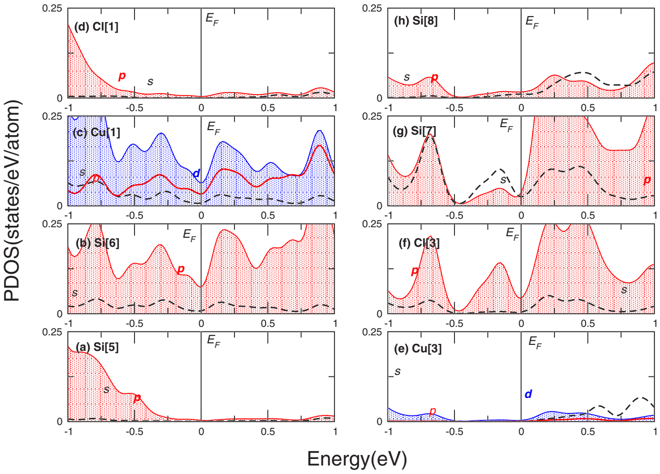

FIG. 9. (Color online) pDOS around the Fermi energy of the $n=3$ superlattice. The pDOS of the interface atoms (Si[4], Cu[1], Cl[2], and Si[5]) and of some of other atoms are shown. (a) Si[5], (b) Si[6], (c) Cu[1], (d) Cl[1], (e) Cu[3], (f) Cl[3], (g) Si[7], and Si[8]. The s orbital pDOS are shown by a black dotted line; the p by a red solid line. For Si and Cl atoms, the area below the pDOS of p orbitals is shown lightly shaded (in red); for Cu atoms, the area below the pDOS of d orbitals is shown heavily shaded (in blue).

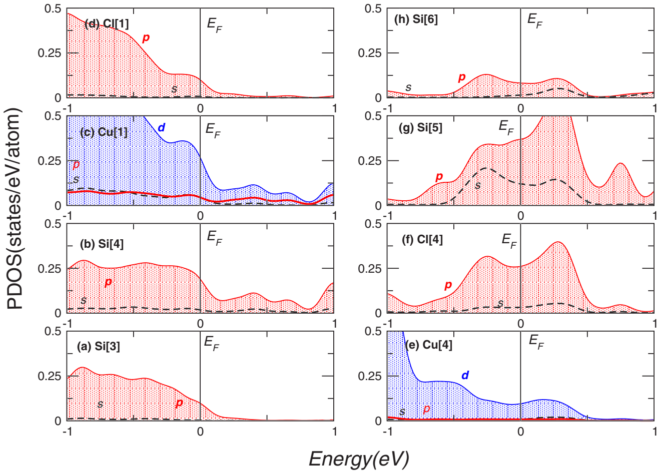

FIG. 10. (Color online) pDOS around the Fermi energy of the 4/12 superlattice. The pDOS of the interface atoms (Si[4], Cu[1], Cl[2], and Si[5]) plus some of other atoms are shown. (a) Si[3], (b) Si[4], (c) Cu[1], (d) Cl[1], (e) Cu[4], (f) Cl[4], (g) Si[5], and Si[6]. The s orbitals are shown in black dotted line; the p by a red solid line. For Si and Cl atoms, the area below the pDOS of p orbitals is shown lightly shaded (in red); for Cu atoms, the area below the pDOS of d is shown heavily shaded (in blue).

C. Density of states

As expected from the band structures, Fermi surfaces, and charge densities, the interface atoms and the other atoms contribute differently to the pDOS at E_F. We present the DOS only of the $n=3$ [111] and 4/12 [001] cases since the trends of the DOS in the other cases [$n=1$ (111) and 2/8, and 4/8 (001)] are the same.

First, in the $n=3$ case, the pDOS of Si[5], Si[6], Cu[1], and Cl[1] are shown in Figs. 9(a)–9(d), which corresponds to the Cu/Si interface; the pDOS of Cu[3], Cl[3], Si[7], and Si[8] are shown in Figs. 9(e)–9(h), which corresponds to the Cl/Si interface. Both Cl[1] and Si[5] have negligible DOS at E_F, while Cu[1] and Si[6] have a strong DOS at E_F. At the Cl/Si interface, Cl[3] and Si[7] have a strong DOS at E_F,

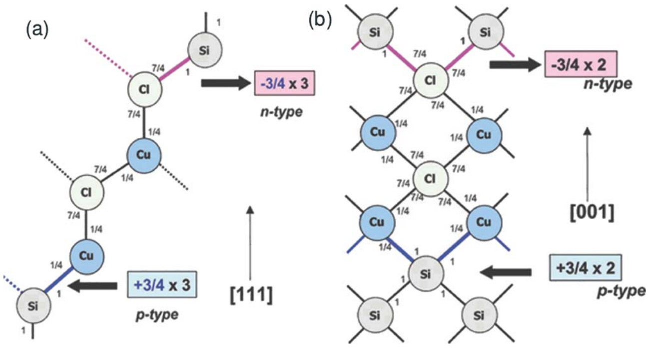

FIG. 11. (Color online) Schematic illustration of bondings in superlattices. (a) [111] superlattice and (b) [001] superlattice. Average number of electrons per bond is shown at each bond. The p-type interface lacks $3/4e^-$ charge per bond and the n-type interface has an excess of $3/4e^-$ electronic charge per bond. In the [111] case, one of bonds off vertical is not shown.

TABLE IV. Relative changes (in %) of the orbital resolved MT charges of the interface atoms in the $n=3$ [111] and 4/12 [001] superlattices with respect to bulk Si and CuCl.

$n=3$	s	p	d	4/12	s	p	d
Si[6]	3.67	−8.18		Si[4]	2.09	−4.97	
Cu[1]	2.10	0.43	−2.02	Cu[1]	1.54	0.21	−1.60
Cl[3]	1.29	−1.01		Cl[4]	0.48	−0.45	
Si[7]	10.55	−14.31		Si[5]	2.96	−3.38	

TABLE V. Calculated electron-phonon coupling constant (λ), Coulomb pseudopotential ($\mu^\star$), and T_C for [111] ($n=1$ and $n=3$) and [001] (2/8, 4/8, and 4/12) superlattices.

	λ	$\mu^\star$	T_C (K)
$n=1$	0.411	0.09	2.09
$n=3$	0.155	0.02	0.03
2/8	0.406	0.05	4.40
4/8	0.253	0.04	0.45
4/12	0.210	0.05	0.06

while those of Cu[3] and Si[8] are negligible.

Second, in the 4/12 [001] case (Fig. 10), the pDOS of Si[3], Si[4], Cu[1], and Cl[1] are shown in (a)–(d), which corresponds to the Cu/Si interface; the pDOS of Cu[4], Cl[4], Si[5], and Si[6], are shown in (e)–(h), which corresponds to the Cl/Si interface. At the Cu/Si interface side, the DOS at E_F in Cu[1] and Si[4] are large, while that in Si[3] is not negligible but smaller than those at the interfaces. The Cl/Si interface exhibits a similar pattern as the Cu/Si interface: the interface atoms (Si[5] and Cl[4]) have a large DOS value at E_F, while the Si[6] has a non-negligible DOS at E_F but is smaller than those at the interfaces. Both Cl[1] and Cu[4], however, as in the $n=3$ case, have negligible DOS at E_F. The non-negligible DOS at E_F of Si atoms (Si[3] and Si[6]) is consistent with the charge density plot: charge is more spread away from the interface to the Si region compared to the [111] superlattice.

D. Interface charge

For the quantitative analysis of interface charge, changes of the MT charge (in %) relative to their bulk counterparts are listed in Table IV for the $n=3$ and 4/12 cases. Interface Si atoms lose their charge while interface Cu and Cl gain charge. In this analysis, only MT charges are considered, while interstitial charge is not taken into account. One thing common in [111] and [001] is that interface Cu loses its d charge but gains s charge while interface Si gains s charge but loses p charge.

While the bonding nature of bulk Si (CuCl) is covalent (ionic), new bondings are formed at the interfaces—as seen in the change of layer distances and charge densities. A schematic bonding is illustrated In Fig. 11 for the (a) [111] and (b) [001] superlattices. Since all atoms are tetrahedrally coordinated, there are four bonds per atom. For simplicity, we present only three arms for the [111] case. According to the two-electron-per-bond counting rule, each atom, Si, Cu, and Cl, has 1, 1/4, and 7/4 electrons per bonding arm, respectively. The Cu-Si arm lacks 3/4 electrons, whereas the Cl-Si arm has an excess of 3/4 electrons. This simple electron counting per bond explains very well why the Cu/Si interface is p type and the Cl/Si interface is n type.

IV. SUPERCONDUCTIVITY

The presence of the 2D metallic states surrounded by dielectric layers can provide an optimal condition close to the model for excitonic superconductivity originally suggested by Little,[9] Ginzburg,[10] and ABB.[11] In fact, the experiment by Mattes and Foiles, where a large diamagnetic signal for epitaxially grown CuCl on a Si [111] substrate was observed between 60 and 150 K, motivates us to first estimate T_C of the CuCl/Si superlattices based on the BCS-type electron-phonon coupling mechanism. Although a 2D formulation of superconductivity would be more appropriate for the present system, it is beyond the scope of this work. In the following, we use a standard three-dimensional approach because it can shed some light on electron-phonon coupling and superconductivity in our system. Thus, we estimate the McMillan-Hopfield[33,34] electron-phonon coupling constant, λ_{ep}, which can be written as $\lambda_{ep}=\Sigma_t \eta_t / M_t \langle \omega^2 \rangle$.[35]

The spherically averaged Hopfield parameter for each atom type, η_t, calculated in the crude RMTA,[27,36] is

$$\eta = 2N(E_F)\sum_l (l+1)M^2_{l,l+1}\frac{f_l f_{l+1}}{(2l+1)(2l+3)}, \tag{1}$$

where $f_l = N_l(E_F)/N(E_F)$ is a fractional pDOS of a given atom and $M_{l,l+1}$ is an electron-phonon matrix element given by

$$M_{l,l+1} = \int_0^R R_l \frac{dV}{dr} R_{l+1} r^2 dr, \tag{2}$$

TABLE VI. Hopfield parameter (η) and the electron-phonon coupling constant (λ) in the $n=1$ superlattice. The total electron-phonon coupling constant, λ_{ep}, is 0.411.

	Si[1]	Si[2]	Cu	Cl	Si[3]	Si[4]
η (eV/Å^2)	0.003	0.036	0.368	0.172	0079	0.007
λ	0.000	0.004	0.271	0.127	0.008	0.000

TABLE VII. Hopfield parameter (η) and the electron-phonon coupling constant (λ) in the $n=3$ superlattice of some interface atoms. The total electron-phonon coupling constant, λ_{ep}, is 0.155.

	Si[6]	Cu[1]	Cl[3]	Si[7]
η (eV/Å^2)	0.048	0.064	0.128	0.042
λ	0.005	0.047	0.094	0.004

TABLE IX. Hopfield parameter (η) and the electron-phonon coupling constant (λ) in the 4/8 superlattice. The total electron-phonon coupling constant, λ_{ep}, is 0.253.

	Si[4]	Cu[1]	Cl[4]	Si[5]	Si[6]	Si[7]
η (eV/Å^2)	0.013	0.014	0.254	0.358	0.024	0.019
λ	0.001	0.010	0.187	0.039	0.003	0.002

with the gradient of the potential and radial functions R_l and R_{l+1} calculated at E_F. According to Pettifor[37] and Glözel *et al.*,[38] Eq. (2) can be rewritten (see also Refs. 36 and 39) as

$$M_{l,l+1} = -\phi_l(E_F)\phi_{l+1}(E_F)\{[D_l(E_F) - l][D_{l+1}(E_F) + l + 2] + [E_F - V(S)]S^2\}, \tag{3}$$

where $V(S)$ is the one-electron potential and $\phi_l(E_F)$ the amplitude of the l partial wave at the sphere boundary (radius $=S$) evaluated at E_F. The average phonon frequency can be estimated by $\langle\omega_t^2\rangle^{1/2}=0.69\Theta_D^t$, where Θ_D^t is the Debye temperature and t is the atom type index. We took experimental values for Θ_D, 625 K for Si (Ref. 40) and 180 K for CuCl,[41] and evaluated the electron-phonon coupling constant as

$$\lambda_{ep} = \sum_{\mathrm{Si}} \frac{\eta(\mathrm{Si})_t}{M_{\mathrm{Si}}\langle\omega_{\mathrm{Si}}^2\rangle} + \sum_t \frac{\eta(\mathrm{Cu})_t + \eta(\mathrm{Cl})_t}{\frac{1}{2}M_{\mathrm{CuCl}}\langle\omega_{\mathrm{CuCl}}^2\rangle}, \tag{4}$$

where the average mass of CuCl was used for Cu and Cl.[42,43] To estimate T_C we used McMillan's formula[33]

$$T_c = \frac{\langle\omega^2\rangle^{1/2}}{1.2}\exp\left[-\frac{1.04(1+\lambda_{ep})}{\lambda_{ep} - \mu^\star(1+0.62\lambda_{ep})}\right]. \tag{5}$$

The average phonon frequency is now evaluated with $\langle\omega^2\rangle^{1/2}=0.69\langle\Theta_D\rangle$, where Θ_D is the weighted average of Θ_D for Si and CuCl. The electron-phonon coupling constant (λ_{ep}), the Coulomb pseudopotential ($\mu^\star$),[44] and T_C of the superlattices are given in Table V. The calculated Hopfield parameters (η) and the electron-phonon coupling constants (λ_t) per atom type are tabulated in Table VI ($n=1$), Table VII ($n=3$), Table VIII (2/8), Table IX (4/8), and Table X (4/12). In the $n=1$ case, all atoms are listed, whereas only the atoms with the largest contribution are listed for the other cases. The $n=1$ (111) and 2/8 (001) cases have $\lambda=0.411$ and 0.406, respectively, which result in T_C to be 2.09 and 4.40 K, respectively. The higher T_C in the 2/8 case is due to the lower value of $\mu^\star$. The other cases ($n=3$, 4/8, and 4/12) have T_C of 0.03, 0.45, and 0.06 K, respectively. In the $n=1$ case, Cu has the largest value of λ and η. For the other cases, on the contrary, λ and η values are small for the interface Cu; the interface Cl atom has the largest value of λ. The interface Cl [2/8] and Si [4/8, 4/12] of the Cl/Si interface have the largest η values. The fact that the interface Cl atom has the largest η value indicates superconductivity is indeed an interface effect in the electron-phonon mediation scheme. In the [111] superlattice, the larger λ value in the interface Cl than the interface Cu in the $n=3$ case, while Cu has a large value in the $n=1$ case, implies that the addition of CuCl and Si layers changes the electron-phonon interaction. Furthermore, the large η and λ values of the interface Cl in the $n=3$ case and the [001] superlattices indicate that it is the Cl/Si interface which plays a more important role for superconductivity. The electron-phonon interaction matrix elements, $M_{l,l+1}$, change very little for a given atom type within a superlattice. The drastic changes of η values [see Eq. (1)] show that the fractional pDOS, f_l's, play the leading role in determining the Hopfield parameters. In particular, the different η values for the same atom kind within a superlattice arise from the gain or loss of charge.

For the other cases, the lower T_C is due to the reduction of the η values, hence smaller values of λ. The DOS contribution of interface atoms, f_l in Eq. (1), gets smaller as the total number of layers increases since there are only two interfaces for any number of layers; therefore the fractional DOS, f_l, of interface atoms also diminishes as the number of layer increases. Furthermore, the McMillan formula used for the T_C estimation is a numerical solution of the "isotropic" Eliashberg equation. However, the electron-phonon coupling in the CuCl/Si superlattices is highly anisotropic; thus, T_C might be higher if anisotropy of the electron-phonon coupling is rigorously taken into account in the T_C estimation.

Regarding experiment, we mentioned in Sec. I that a nearly ideal diamagnetic signal believed to be due to superconductivity was observed between 60 and 150 K in CuCl

TABLE VIII. Hopfield parameter (η) and the electron-phonon coupling constant (λ) in the 2/8 superlattice. The total electron-phonon coupling constant, λ_{ep}, is 0.406.

	Si[4]	Cu[1]	Cl[2]	Si[5]	Si[6]	Si[7]	Si[8]
η (eV/Å^2)	0.023	0.028	0.458	0.303	0.010	0.012	0.014
λ	0.002	0.020	0.338	0.033	0.001	0.001	0.001

TABLE X. Hopfield parameter (η) and the electron-phonon coupling constant (λ) in the 4/12 superlattice. The total electron-phonon coupling constant, λ_{ep}, is 0.210.

	Si[4]	Cu[1]	Cl[1]	Cl[4]	Si[5]	Si[6]	Si[7]
η (eV/Å^2)	0.019	0.037	0.020	0.161	0.206	0.015	0.016
λ	0.002	0.027	0.015	0.119	0.022	0.002	0.002

over Si [111].[20] Thus if this system is superconducting as speculated by Mattes and Foiles, our investigation indicates that the electron-phonon interaction alone would not be able to account for it. In this sense, to study superconductivity further on these superlattices, the electronic (or excitonic) mechanism needs to be pursued.

ACKNOWLEDGMENTS

We are grateful to C. W. Chu, A. A. Abrikosov, and J. B. Ketterson for their encouragement and fruitful discussions, the early encouragement of J. Bardeen, and to M. Weinert, J. H. Lee, and I. G. Kim for technical comments. This work was supported by the Department of Energy (Grant No. DE-FG02-88ER 45372/A021) and a supercomputing time grant at the NERSC.

---

*sonny@pluto.phys.northwestern.edu

[1] G. A. Baraff, J. A. Appelbaum, and D. R. Hamann, Phys. Rev. Lett. **38**, 237 (1977).

[2] W. A. Harrison, E. A. Kraut, J. R. Waldrop, and R. W. Grant, Phys. Rev. B **18**, 4402 (1978).

[3] R. W. Grant, J. R. Waldrop, and E. A. Kraut, Phys. Rev. Lett. **40**, 656 (1978).

[4] T. Wang, N. Moll, K. Cho, and J. D. Joannopoulos, Phys. Rev. Lett. **82**, 3304 (1999).

[5] A. Ohtomo, D. A. Muller, J. L. Grazul, and H. Y. Hwang, Nature (London) **419**, 378 (2002).

[6] S. Okamoto and A. J. Millis, Nature (London) **428**, 630 (2004).

[7] A. Ohtomo and H. Y. Hwang, Nature (London) **427**, 423 (2004).

[8] S. Okamoto and A. J. Millis, Physica B **359**, 1378 (2005).

[9] W. Little, Phys. Rev. **134**, A1416 (1964).

[10] V. L. Ginzburg, Zh. Eksp. Teor. Fiz. **47**, 2318 (1964) [Sov. Phys. JETP **20**, 1549 (1965)]; Phys. Lett. **13**, 101 (1964).

[11] D. Allender, J. Bray, and J. Bardeen, Phys. Rev. B **7**, 1020 (1973).

[12] D. L. Miller, M. Strongin, O. F. Kammerer, and B. G. Streetman, Phys. Rev. B **8**, 4416 (1973).

[13] M. Strongin, O. F. Kammerer, H. H. Farrell, and D. L. Miller, Phys. Rev. Lett. **30**, 129 (1973).

[14] C. C. Tsuei and W. L. Johnson, Phys. Rev. B **9**, 4742 (1974).

[15] D. L. Miller, M. Strongin, O. F. Kammerer, and B. G. Streetman, Phys. Rev. B **13**, 4834 (1976).

[16] N. B. Brandt, S. V. Kuvshinnikov, A. P. Rusakov, and V. M. Semenov, JETP Lett. **27**, 33 (1978).

[17] C. W. Chu, A. P. Rusakov, S. Huang, S. Early, T. H. Geballe, and C. Y. Huang, Phys. Rev. B **18**, 2116 (1978).

[18] A. A. Abrikosov, Pis'ma Zh. Eksp. Teor. Fiz. **27**, 235 (1978) [JETP Lett. **27**, 219 (1978)].

[19] A. A. Abrikosov, J. Less-Common Met. **62**, 451 (1978).

[20] B. Mattes and C. Foiles, Physica B & C **135B**, 139 (1985).

[21] B. Mattes, Physica C **162-164**, 554 (1989).

[22] J. J. Yu and A. J. Freeman, Army Research Conference, NJ, 15 December 1986 (unpublished).

[23] In the $n=2$ [111] superlattice, we found that Cu and Cl inside CuCl region have their positions interchanged during the geometry optimization. Thus, we exclude the $n=2$ case in this paper.

[24] n is an integer and m is an even integer. $2n+m$ should be a multiple of 4 to satisfy the periodicity along the [001] direction.

[25] E. Wimmer, H. Krakauer, M. Weinert, and A. J. Freeman, Phys. Rev. B **24**, 864 (1981).

[26] H. J. F. Jansen and A. J. Freeman, Phys. Rev. B **30**, 561 (1984).

[27] G. Gaspari and B. Gyorffy, Phys. Rev. Lett. **28**, 801 (1972).

[28] In the [001] superlattice, the first four layers are labeled as Si[1], Si[2], Si[3], and Si[4]. We put CuCl layers on top of the first four Si layers and then put the rest of the Si layers on the CuCl layers.

[29] For the [001] superlattice, $(\mathrm{CuCl})_n/(\mathrm{Si})_m$ is simply denoted as n/m.

[30] L. Hedin and B. Lundqvist, J. Phys. C **4**, 2064 (1971).

[31] P. E. Blöchl, O. Jepsen, and O. K. Andersen, Phys. Rev. B **49**, 16223 (1994).

[32] The a used for the comparison is 5.43 Å.

[33] W. McMillan, Phys. Rev. **167**, 331 (1968).

[34] J. Hopfield, Phys. Rev. **186**, 443 (1969).

[35] H. G. Salunke, R. Mittal, G. P. Das, and S. L. Chaplot, J. Phys.: Condens. Matter **9**, 10137 (1997).

[36] H. L. Skriver and I. Mertig, Phys. Rev. B **32**, 4431 (1985).

[37] D. G. Pettifor, J. Phys. F: Met. Phys. **7**, 1009 (1977).

[38] D. Glözel, D. Rainer, and H. R. Schober, Z. Phys. B **35**, 317 (1979).

[39] H. L. Skriver and I. Mertig, Phys. Rev. B **41**, 6553 (1990).

[40] N. W. Ashcroft and N. D. Mermin, *Solid State Physics* (Holt, Rinehart and Winston, New York, 1976).

[41] Z. Vardeny, G. Gilat, and D. Moses, Phys. Rev. B **18**, 4487 (1978).

[42] *High-Temperature Superconductivity*, edited by V. L. Ginzburg and D. A. Kirzhnits (Consultants Bureau, New York, 1977).

[43] There are several choices of evaluating λ from the individual Hopfield parameters. For compounds, we follow the way suggested in Ref. 42. Furthermore, CuCl is regarded as one entity in vibration.

[44] K. Bennemann and J. Garland, in *Superconductivity in d- and f-band Metals*, AIP Conf. Proc. No. 3, edited by D. H. Douglas (AIP, New York, 1972), p. 103.